

The energy budget for X-ray to infrared reprocessing in Compton-thin and Compton-thick active galaxies

Tahir Yaqoob¹ and Kendrah D. Murphy²

¹Department of Physics and Astronomy, Johns Hopkins University, Baltimore, MD 21218.

²Department of Physics, Skidmore College, 815 North Broadway, Saratoga Springs, NY 12866.

Accepted 2010 October 28. Received Received 2010 October 27; in original form 2010 September 21.

ABSTRACT

Heavily obscured active galactic nuclei (AGNs) play an important role in contributing to the cosmic X-ray background (CXRb). However, the AGNs found in deep X-ray surveys are often too weak to allow direct measurement of the column density of obscuring matter. One method adopted in recent years to identify heavily obscured, Compton-thick AGNs under such circumstances is to use the observed mid-infrared to X-ray luminosity ratio as a proxy for the column density. This is based on the supposition that the amount of energy lost by the illuminating X-ray continuum to the obscuring matter and reprocessed into infrared emission is directly related to the column density and that the proxy is not sensitive to other physical parameters of the system (aside from contamination by dust emission from, for example, star-forming regions). Using Monte Carlo simulations, we find that the energy losses experienced by the illuminating X-ray continuum in the obscuring matter are far more sensitive to the shape of the X-ray continuum and to the covering factor of the X-ray reprocessor than they are to the column density of the material. Specifically we find that it is possible for the infrared to X-ray luminosity ratio for a Compton-thin source to be just as large as that for a Compton-thick source *even without any contamination from dust*. Since the intrinsic X-ray continuum and covering factor of the reprocessor are poorly constrained from deep X-ray survey data, we conclude that the mid-infrared to X-ray luminosity ratio is not a reliable proxy for the column density of obscuring matter in AGNs even when there is no other contribution to the mid-infrared luminosity aside from X-ray reprocessing. This conclusion is independent of the geometry of the obscuring matter.

Keywords: galaxies: active - radiation mechanism: general - scattering - X-rays: galaxies – infrared: galaxies

1 INTRODUCTION

Although it has been known since the 1980s that a significant fraction of the active galactic nuclei (AGNs) that contribute to the CXRB X-ray background (CXRb) must be heavily absorbed (Setti & Woltjer 1989), the details of the absorbed population remain uncertain (e.g., Comastri et al. 1995; Tozzi et al. 2006; Polletta et al. 2006; Gilli, Comastri, & Hasinger 2007; Frontera et al. 2007; Martínez-Sansigre et al. 2007; Ballantyne & Papovich 2009; Treister, Urry, & Virani 2009; Draper & Ballantyne 2009; Fiore et al. 2009; Georgantopoulos et al. 2008, 2009; Malizia et al. 2009, 2010). One of the reasons for this is that the problem is highly degenerate. Another reason is that, although much progress has been made in the last decade or so in resolving the hard X-ray background below 10 keV, the bulk of the resolved AGNs are too weak to robustly measure their column densities with X-ray spectroscopy. As a result, a number of indirect “proxies” have come into use for interpreting deep survey data and identifying heavily obscured AGNs. One of these is the use of the equivalent width (EW) of the Fe K α line at ~ 6.4 keV as a rough indicator of the column density because EWs larger than ~ 1 keV cannot be produced by a Compton-thin X-ray reprocessor (e.g., see Ghisellini, Haardt, & Matt 1994; Ikeda, Awaki, & Terashima 2009; Murphy & Yaqoob 2009, hereafter MY09). However, AGNs found in deep surveys are seldom bright enough to allow a direct robust

2 Tahir Yaqoob & Kendrah D. Murphy

measurement of the Fe K α line EW. An additional constraint could in principle be obtained from an independent indicator of the intrinsic AGN continuum luminosity such as an emission line in a different waveband. A few have been explored, the ratio of the luminosity of [O III] λ 5007Å luminosity to the observed X-ray luminosity being the oldest (e.g., Maiolino et al. 1998; Bassani et al. 1999; Zakamska et al. 2003; Cappi et al. 2006; Panessa et al. 2006; Reyes et al. 2008; Bongiorno et al. 2010). Meléndez et al. (2008) have explored the use of the ratio of the luminosity of the [O VI] λ 25.89 μ m emission line to the observed X-ray luminosity as a diagnostic of the column density. Gilli et al. (2010) have recently suggested the analogous use of the [Ne V] λ 3426Å emission line. However, derivation of the column density from these indicators is highly model-dependent as there are degenerate solutions (in addition to uncertainties in calibration of the relations), and even then, the method can only give a line-of-sight column density, which may be different to that out of the line-of-sight. A third indicator that is used to identify heavily obscured AGNs in deep X-ray surveys is the ratio of the mid-infrared luminosity to the *observed* X-ray luminosity (e.g., Martínez-Sansigre et al. 2005; Daddi et al. 2007; Hickox et al. 2007; Alexander et al. 2008; Fiore et al. 2008, 2009; Georgantopoulos et al. 2008, 2009, 2010; Vignali et al. 2010; Bauer et al. 2010; Georgakakis et al. 2010, and references therein). The idea is that the intrinsic AGN continuum that intercepts the obscuring matter loses energy due to the absorption and Compton-scattering of X-ray photons and that this energy loss ultimately heats the medium so that it is then reradiated in the infrared band. It is then supposed that the ratio of the infrared to observed X-ray luminosity in AGNs could be an indicator of the column density of the reprocessor. Since reprocessed emission from dust can also provide a significant contribution to the infrared band (e.g., Maiolino et al. 2007; Horst et al. 2008; Rowan-Robinson, Valtchanov, & Nandra 2009; Georgakakis et al. 2010), it has certainly been recognized that interpretation of the mid-infrared to X-ray luminosity ratio indicator is complex. Nevertheless, it is still believed (e.g., Mullaney et al. 2010, and references therein) that it will eventually be possible to discriminate between different scenarios and utilize the mid-infrared to X-ray luminosity ratio to identify Compton-thick AGNs. In the meantime, whilst an unusually large mid-infrared to X-ray luminosity ratio does not necessarily mean that an AGN is heavily obscured, an *unusually small* ratio could (it is supposed) be used to establish that an AGN is *not* a candidate to be a Compton-thick source. In other words, rejection of Compton-thick candidates may also be useful.

Unfortunately it has never been demonstrated, even without the complications arising from dust emission, that the mid-infrared emission to X-ray luminosity ratio should be sensitive to the X-ray absorbing column density to the extent that the ratio could be used to infer the magnitude of that column density. One cannot correct for the effects of dust if the relation between the X-ray energy reprocessed into the infrared band has not been quantified theoretically. It is the aim of the present paper to investigate and quantify the relationship between the energy lost by the intrinsic X-ray continuum in the obscuring matter and the column density of that reprocessor, *explicitly without the complications of dust emission*. Calculating the energy available from X-ray losses for reemission in the mid-infrared band is of course only the first step in the process. However, establishing that the energy budget from X-ray losses is sensitive to the column density, and *not* sensitive to other key parameters, is a *minimal* requirement for the mid-infrared to X-ray luminosity ratio to be a useful indicator of the column density. If we find, as we do, that this minimal requirement is not met, then additional physical processes can only *lessen* the usefulness of the diagnostic. Our investigation is based upon the toroidal X-ray reprocessor model of MY09, but our principal conclusions will have general applicability and will be independent of geometry.

The paper is organized as follows. In §2 we give a brief overview of the assumptions of the MY09 model and describe the method we used to analyze the energy budget. In §3 we present the results of X-ray energy losses in the reprocessor as a function of injection energy, and in §4 we present the results of integrating these “loss” spectra over an incident power-law continuum. It is in §4 that we show the relationship between the integrated energy loss and the column density of the obscuring matter, as well as the dependence of the energy losses on the covering factor and on the power-law spectral index. In §5 we define a proxy for the ratio of the infrared luminosity due to X-ray energy losses, to observed X-ray luminosity and present the results of computations of this ratio as a function of the column density of obscuring matter. We summarize our conclusions in §6.

2 METHOD

Here we give a brief overview of the critical assumptions that our model Monte Carlo simulations are based upon. Full details can be found in MY09. Our geometry is an azimuthally-symmetric doughnut-like torus with a circular cross-section, characterized by only two parameters, namely the half-opening angle, θ_0 , and the equatorial column density, N_H (see Fig. 1 in MY09). We assume that the X-ray source is located at the center of the torus and emits isotropically and that the reprocessing material is uniform and essentially neutral (cold). For illumination by an X-ray source that is emitting isotropically, the mean column density, integrated over all incident angles of rays through the torus, is $\bar{N}_H = (\pi/4)N_H$. The inclination angle between the observer’s line of sight and the symmetry axis of the torus is given by θ_{obs} , where $\theta_{\text{obs}} = 0^\circ$ corresponds to a face-on observing angle and $\theta_{\text{obs}} = 90^\circ$ corresponds to an edge-on observing angle. In our calculations we distribute the emergent

photons in 10 angle bins between 0° and 90° that have equal widths in $\cos \theta_{\text{obs}}$, and refer to the face-on bin as #1, and the edge-on bin as #10 (see Table 1 in MY09).

We used a version of our Monte Carlo code that injects single photons (as opposed to bundles of photons, with weights), so that energy is explicitly conserved in the code. Photons were injected with energies in the range 5–500 keV. In the present study we are interested in the energy losses and not the emergent spectra so for energies below 5 keV we calculated energy losses for absorption only, since the relative contribution from Compton scattering is negligible in this regime. If the solid angle subtended by the torus at the X-ray source is $\Delta\Omega$, the covering factor is $[\Delta\Omega/(4\pi)] = 1 - \cos \theta_{\text{obs}}$ (θ_{obs} only varies between 0° and 90°). The covering factor may also be expressed in terms of the physical dimensions of the torus. If a is the radius of the circular cross-section of the torus, and $c + a$ is the equatorial radius of the torus then $[\Delta\Omega/(4\pi)] = (a/c)$ (see MY09). Our model employs a full relativistic treatment of Compton scattering, using the full differential and total Klein-Nishina Compton-scattering cross-sections. We utilized photoelectric absorption cross-sections for 30 elements as described in Verner & Yakovlev (1995) and Verner et al. (1996) and we used Anders and Grevesse (1989) elemental cosmic abundances in our calculations. The Fe K α , Fe K β , and Ni K α fluorescent emission lines were included in the model, as described in MY09. We performed Monte Carlo simulations for (a/c) in the range 0.1–1.0 and N_{H} in the range $3 \times 10^{22} \text{ cm}^{-2}$ to 10^{25} cm^{-2} .

3 ENERGY LOSS SPECTRA

For photons injected into the torus with an energy E , in the interval dE , we define $D[(a/c), N_{\text{H}}, E]dE$ as the fractional energy lost by those photons due to X-ray absorption and Compton downscattering in the torus. This is shown symbolically in equation 1, where $F_{\text{absorbed}}(E)$ and $F_{\text{C}}(E)$ are fractions of the original energy E that are ultimately absorbed or lost to the medium through Compton downscattering respectively. N_0 is the number of photons injected but obviously cancels out of the definition. The function D does not of course only depend on (a/c) , N_{H} , and E , it depends on many other factors such as element abundances and geometry. A photon that undergoes Compton scattering is ultimately either absorbed or escapes the medium. However, absorption can result in line emission and such line photons either escape ($F_L(E)$ in equation 1) or are themselves absorbed.

$$\begin{aligned} D[(a/c), N_{\text{H}}, E] &\equiv \frac{N_0 E [F_{\text{absorbed}}(E) + F_{\text{C}}(E) - F_L(E)]}{N_0 E} \\ &= \int_0^E [1 - F_{\text{escape}}(E, E')] dE' \end{aligned} \quad (1)$$

In practice, using our Monte Carlo code we can track photons injected in a given energy interval and count the energy that escapes. The energy that does not escape must have been given up to the reprocessing medium and this is represented in the second part of equation 1. Whereas the functions $F_{\text{absorbed}}(E)$, $F_{\text{C}}(E)$, and $F_L(E)$ are already integrated over the energy distribution resulting from a single injection energy, E , the function $F_{\text{escape}}(E, E')$ in equation 1 needs to be explicitly integrated over the distribution of downscattered energies, from 0 to E . We also summed over all escaping angles since we are interested in the total energy lost to the medium. Our model includes only three emission lines so we miss some of the escaping energy and therefore overestimate the energy loss, which is already just an upper limit on the total energy available for reprocessing into infrared emission. Moreover, our conclusions in the present paper will not be affected by neglect of the energy in the omitted emission lines. Note that if the torus were completely opaque and non-reflective at all energies, $D[(a/c), N_{\text{H}}, E]$ would simply be equal to (a/c) , the covering factor, since that is the fraction of the energy that would be intercepted and lost to the torus.

In Fig. 1 we show curves of the quantity $D[(a/c), N_{\text{H}}, E] / (a/c)$ for five different column densities in range $3 \times 10^{22} \text{ cm}^{-2}$ to 10^{25} cm^{-2} (solid, black curves), computed from our Monte Carlo simulations. The curves have been calculated for $(a/c) = 0.5$ but have then been normalized by the covering factor, (a/c) . The purpose of this is to later facilitate direct comparison of the shapes of the curves for different values of (a/c) . The units for the curves are fractional energy loss per unit energy, per unit covering factor. We see that at low energies, below ~ 1 keV, the fractional energy loss per keV has already reached its limiting value of (a/c) for all of the column densities shown. At higher injection energies less of the energy is lost but the threshold for it to drop below (a/c) depends on N_{H} . For the two highest values of N_{H} shown ($5 \times 10^{24} \text{ cm}^{-2}$ and 10^{25} cm^{-2}), this energy loss drops below the maximum only above ~ 10 keV. The drop in the curves in Fig. 1 due to the decrease in absorption with increasing photon injection energy for each N_{H} is followed by a flattening again and then a rise as the energy losses due to Compton downscattering become important. For the two lowest column densities in Fig. 1 we have illustrated how Compton downscattering losses compare with absorption by overlaying the equivalent curves for pure absorption only (red curves).

We found that the normalized functions $D[(a/c), N_{\text{H}}, E] / (a/c)$ could not be distinguished in magnitude or shape (within the statistical errors of the Monte Carlo results) for any value (a/c) in the range 0.1–1.0 for column densities up to 10^{24} cm^{-2} . For higher column densities a dependence of the magnitude and shape of the fractional energy loss curves on the covering factor does become apparent. This is shown in Fig. 2, which shows the curves in Fig. 1 for $N_{\text{H}} = 5 \times 10^{24} \text{ cm}^{-2}$ and 10^{25} cm^{-2} ,

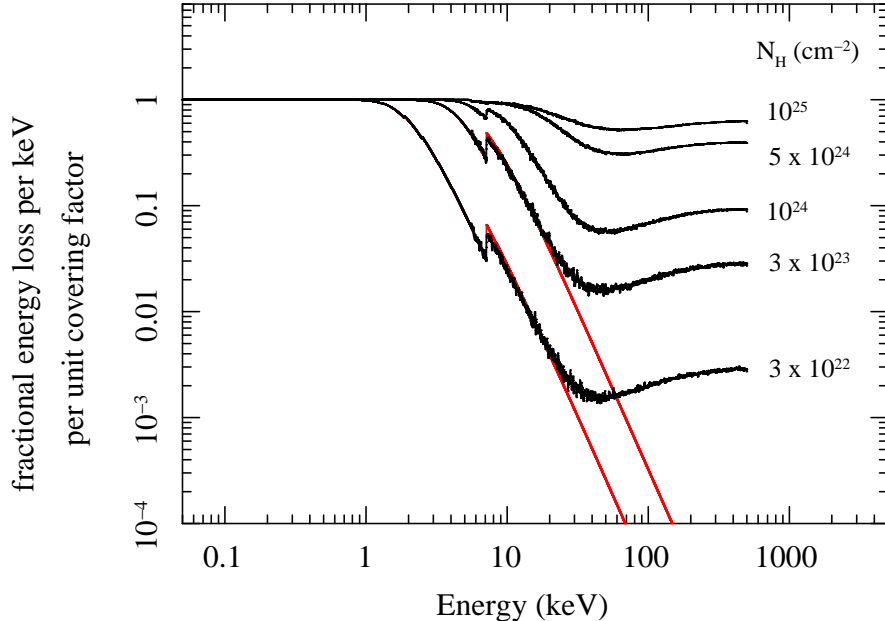


Figure 1. Curves of $D[(a/c), N_H, E]$ (see equation 1), showing the difference between the energy escaping the torus and incident energy (per keV), as a fraction of the incident energy (per keV). The horizontal axis corresponds to the incident energy. The curves were calculated for a covering factor of $[\Delta\Omega/(4\pi)] = (a/c) = 0.5$ but they are normalized by the covering factor so that they can be directly compared with curves with different covering factors (e.g., see Fig. 2). The black curves show the Monte Carlo results for five different column densities, N_H , as shown. The red curves show, for comparison, the effect of neglecting Compton scattering (i.e. for the case of absorption only) for the two lowest column densities.

zoomed in on the region in which Compton scattering dominates. The black curves show the previous results with $(a/c) = 0.5$ and the red and brown curves correspond to $(a/c) = 0.1$ and $(a/c) = 1.0$ respectively. The dependence on covering factor in the Compton-thick regime arises because the amount of energy reflected from the inner surface of the torus and intercepted by the torus again depends on the opening angle of the torus and therefore on the covering factor.

The fractional energy loss curves in Fig. 1 and Fig. 2 do not depend on the shape of the incident X-ray continuum spectrum because the curves give the *fractional* energy loss for monoenergetic photon injection. In order to calculate the absolute energy losses the curves must be multiplied by the incident continuum energy spectrum, as in equation 2 (where A is an arbitrary flux normalization). Since the intrinsic X-ray continuum of AGNs can typically be characterized by a power law with a photon index, Γ , in the range 1.5–2.5, we can expect that the energy losses due to Compton downscattering compared to absorption will be diminished more for steeper spectra than for flatter spectra.

$$L[(a/c), N_H, E] = D[(a/c), N_H, E] A E^{-\Gamma+1} \quad \text{keV cm}^{-2} \text{ s}^{-1} \text{ keV}^{-1} \quad (2)$$

4 CUMULATIVE AND TOTAL ENERGY LOST

So far we have examined the energy losses for monoenergetic injection. We now examine the energy losses integrated over a range of energy. We define the cumulative energy loss, $CL[(a/c), N_H, \Gamma, E]$ for a power-law incident photon spectrum of the form $A E^{-\Gamma}$, between a lower energy, E_L and an energy E , as a fraction of the total incident energy in the energy range E_L to some upper energy, E_U . Thus, we have

$$CL[(a/c), N_H, \Gamma, E] = \frac{\int_{E_L}^E L[(a/c), N_H, E] dE}{\int_{E_L}^{E_U} E^{-\Gamma+1} dE}. \quad (3)$$

The absolute normalization of the incident continuum of course cancels out in equation 3. In the remainder of this paper we use $E_L = 0.5$ keV and $E_U = 500$ keV. The cumulative fractional energy loss function as defined in equation 3 is useful

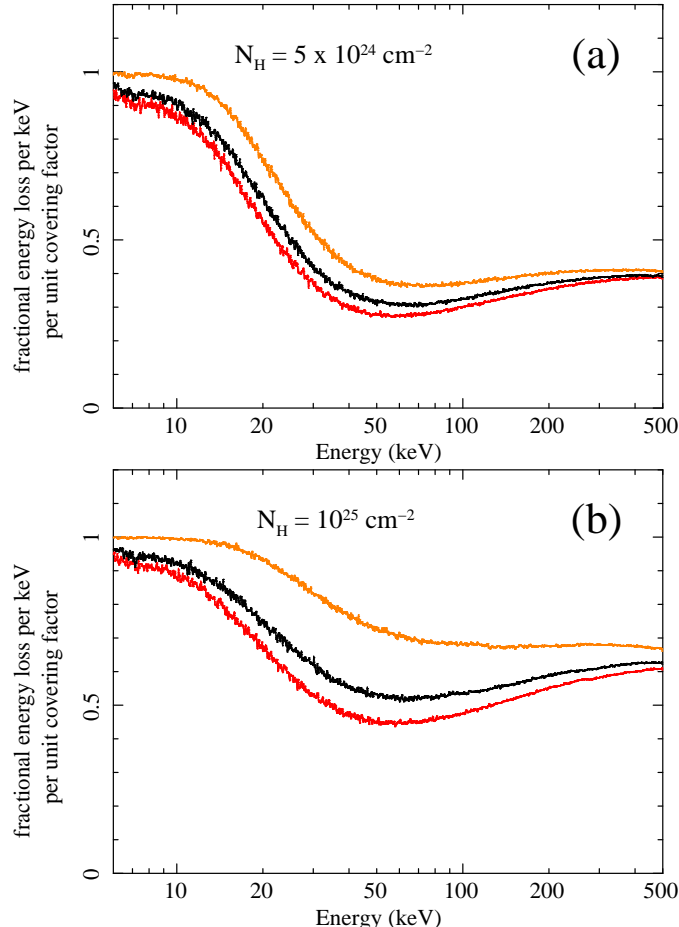


Figure 2. The dependence of the energy loss functions, $D[(a/c), N_H, E]$, on the covering factor, $[\Delta\Omega/(4\pi)] = (a/c)$. Shown are curves for the two highest column densities in Fig. 1, $N_H = 5 \times 10^{24} \text{ cm}^{-2}$ and 10^{25} cm^{-2} . The dependence on (a/c) for $N_H = 10^{24} \text{ cm}^{-2}$ is negligible compared to the statistical errors. Each curve has been normalized to the particular value of (a/c) for that curve in order to facilitate comparison of the *shape* of the functions. The values of the covering factor, (a/c) , in both (a) and (b) are 0.1 (red), 0.5 (black), and 1.0 (brown).

for showing the energy range over which energy losses are most important (for a given set of the parameters (a/c) , N_H , and Γ). In Fig. 3 we show calculations of the function $CL[(a/c), N_H, \Gamma, E]$ in equation 3 for a covering factor of 0.5 and three different values of Γ (1.5, 1.9, and 2.5), each for two different values of N_H (red curves correspond to $3 \times 10^{22} \text{ cm}^{-2}$ and black curves correspond to 10^{25} cm^{-2}). These two extreme column densities correspond to equatorial Thomson depths of the torus of ~ 0.024 and ~ 8.1 for the smaller and larger column respectively, and are therefore representative of a Compton-thin and a Compton-thick case respectively. In Fig. 3, the total energy loss in the range 0.5–500 keV as a fraction of the total incident energy in the same energy band can be read off from the curves at $E = 500$ keV.

Two results are immediately apparent from Fig. 3. The first is that changing the column density by a factor of more than 300, from $3 \times 10^{22} \text{ cm}^{-2}$ to 10^{25} cm^{-2} produces a disproportionately small change in the total integrated fractional energy loss, $CL[(a/c), N_H, \Gamma, E_U]$. For $\Gamma = 2.5$ the change in CL is *only 14% for more than two orders of magnitude change in the column density*. For $\Gamma = 1.9$ and 1.5 the change in CL between the two column densities is only a factor of ~ 2.5 and ~ 11 respectively. The latter still falls short by two orders of magnitude for the change in CL to be commensurate with the change in N_H . The second result that is apparent from Fig. 3 is that for $\Gamma = 2.5$ most of the incident energy has been deposited in the torus below 10 keV, and the incident X-ray continuum above 10 keV makes an insignificant contribution. On the other hand, for $\Gamma = 1.5$, most of the energy is deposited *above* 10 keV. This is because the shape of the incident spectrum is critical on determining whether absorption or Compton scattering dominates the energy losses. Steeper spectra have relatively more photons at lower energies than flatter spectra so absorption is correspondingly more important for steeper spectra. In fact, Fig. 3 shows that the total integrated energy loss for $\Gamma = 2.5$ is larger for the smaller column density than it is for both $\Gamma = 1.5$ and $\Gamma = 1.9$ for the *larger* column density. In other words, the energy loss for the $\Gamma = 2.5$ *Compton-thin case* is larger than the *Compton-thick case* for $\Gamma = 1.5$ and $\Gamma = 1.9$. Finally, we also show in Fig. 3 the result (dotted line) for $\Gamma = 1.9$

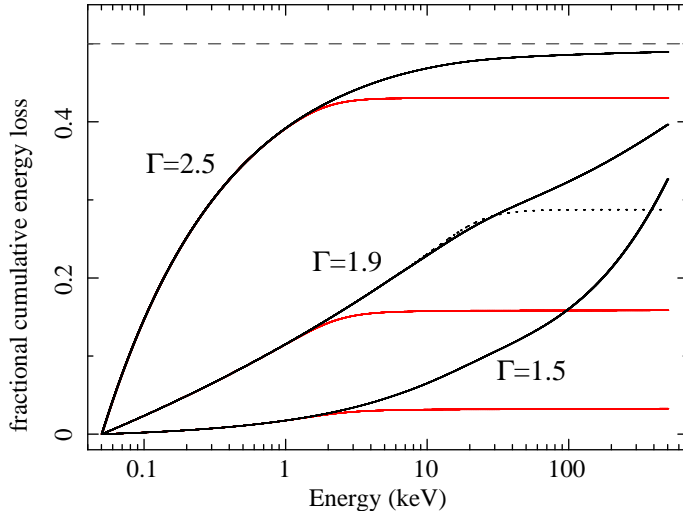


Figure 3. The cumulative fractional energy loss in the torus as a function of energy (i.e. from curves such as those in Fig. 1, integrated from 0.05 keV up to an energy, E ; see equation 3). Pairs of curves are shown for a given incident power-law photon index (Γ), for two column densities: $3 \times 10^{22} \text{ cm}^{-2}$ (red) and 10^{25} cm^{-2} (black). Three pairs of curves are shown, corresponding to $\Gamma = 1.5, 1.9$, and 2.5 . The largest value that any of the curves can possibly have is equal to the covering factor, $[\Delta\Omega/(4\pi)] = (a/c)$, corresponding to *all* the energy intercepted by the torus being captured. These calculations were done for $(a/c) = 0.5$ and this value is shown by the gray dashed line. The dotted curve shows the effect of ignoring Compton scattering for the case of $\Gamma = 1.9$ and $N_H = 10^{25} \text{ cm}^{-2}$ (i.e. pure absorption).

when Compton scattering is neglected (i.e. absorption only). It can be seen that for $\Gamma = 1.9$, Compton scattering increases the energy loss by $\sim 40\%$ compared to the case of absorption only.

4.1 Dependence on column density

In this section we examine the explicit dependence of the total integrated fractional energy loss, $CL[(a/c), N_H, \Gamma, E_U]$, on N_H . Fig. 4 shows this dependence for three values of Γ (1.5, 1.9, and 2.5) and for each of these three values of Γ two curves are shown, corresponding to two values of the covering factor, $(a/c) = 0.1$ (dotted) and $(a/c) = 1.0$ (solid). Note that the quantity that is actually plotted in Fig. 4 is $CL[(a/c), N_H, \Gamma, E_U]/(a/c)$, the total integrated fractional energy loss per unit covering factor. The reason for this is to facilitate a direct comparison of the *shapes* of the curves for different covering factors. We see from Fig. 4 that for $\Gamma = 2.5$, the shape of the total energy loss curves as a function of N_H does not depend on the covering factor. For flatter spectra there is some dependence that develops for column densities greater than $\sim 10^{24} \text{ cm}^{-2}$ but even for $\Gamma = 1.5$ the difference between the $(a/c) = 0.1$ and $(a/c) = 1.0$ curves is no more than $\sim 25\%$ at the highest column density (10^{25} cm^{-2}).

The most important result that Fig. 4 shows is, as already discussed above for Fig. 3, the very different behavior of the energy loss functions as a function of N_H for different values of Γ . For the steepest incident X-ray continuum with $\Gamma = 2.5$, the sensitivity of $CL[(a/c), N_H, \Gamma, E_U]$ to N_H is less than 20% for *a factor of ~ 330 change in N_H* . This is because for such a steep spectrum most of the energy is in the soft X-ray band, and photons with such low energies are readily absorbed by small column densities. Adding more column density then cannot make much difference to the energy loss functions if the bulk of the energy has already been deposited in the torus. Fig. 4 shows that even for $\Gamma = 1.5$, the change in $CL[(a/c), N_H, \Gamma, E_U]$ as N_H changes by a factor of ~ 330 is only just over an order of magnitude. Overall, Fig. 4 shows that the total integrated fractional energy loss is actually not very sensitive to N_H for any value of Γ or (a/c) .

4.2 Dependence on covering factor

In this section we examine the dependence of the total, integrated fractional energy loss, $CL[(a/c), N_H, \Gamma, E_U]$ on the covering factor, (a/c) . Fig. 5 shows curves of the total integrated fractional energy loss versus (a/c) , for five different column densities in the range $3 \times 10^{22} \text{ cm}^{-2}$ to 10^{25} cm^{-2} , calculated for $\Gamma = 1.9$. It can be seen that the relationship between $CL[(a/c), N_H, \Gamma, E_U]$ and (a/c) for a given value of N_H is very simple. In fact, as might be expected, the relationship is linear for the $N_H = 10^{24} \text{ cm}^{-2}$ curve and for the curves with smaller column densities, but there is little departure from linearity even for the $N_H = 10^{25} \text{ cm}^{-2}$ curve. The approximate linearity of $CL[(a/c), N_H, \Gamma, E_U]$ as a function of (a/c) even in the Compton-thick regime is true for any Γ in the range relevant to the present study (range 1.5–2.5). The significance of this result is that, since we have already seen that the dependence of $CL[(a/c), N_H, \Gamma, E_U]$ on N_H can be very weak (much weaker than linear), we can expect the

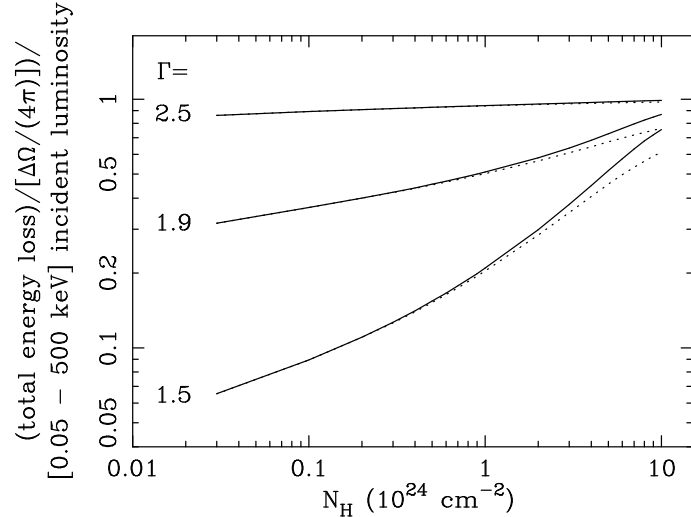


Figure 4. The total 0.05–500 keV integrated energy loss in the torus as a fraction of the total integrated energy in the same bandpass, as a function of the torus equatorial column density, N_H . Three pairs of curves are shown, corresponding to photon indices of the incident power-law spectrum, Γ , of 1.5, 1.9, and 2.5. Each pair corresponds to two different values of the covering factor, $[\Delta\Omega/(4\pi)] = (a/c)$, of 0.1 (dotted) and 1.0 (solid). The curves have been divided by the covering factor in order to facilitate a direct comparison of the *shape* of each pair of curves. The functional dependence on N_H does not vary significantly with (a/c) .

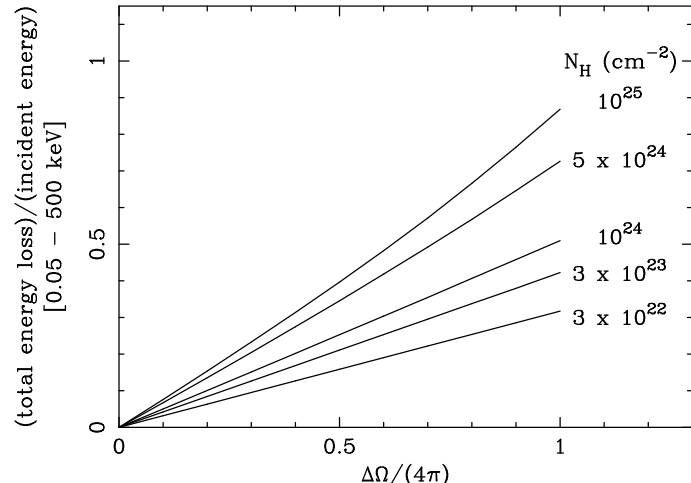


Figure 5. The total 0.05–500 keV integrated energy loss in the torus as a fraction of the total integrated energy in the same bandpass, as a function of the covering factor, $[\Delta\Omega/(4\pi)] = (a/c)$. Curves are shown for five different column densities, as indicated, for an incident power-law photon index of $\Gamma = 1.9$. It can be seen that the total integrated fractional energy loss is approximately a linear function of the covering factor.

covering factor to play a role in the reprocessing of X-rays to infrared emission that is at least, if not more important, than that of the column density.

4.3 Dependence on photon index

In this section we examine the explicit dependence of the total integrated fractional energy loss, $CL[(a/c), N_H, \Gamma, E_U]$, on the photon index of the incident power-law continuum, Γ . Fig. 6 shows this dependence for five different column densities in the range $3 \times 10^{22} \text{ cm}^{-2}$ to 10^{25} cm^{-2} , for $(a/c) = 0.5$ (solid curves), as Γ varies from 1.4 to 2.6. Also shown in Fig. 6 are curves for $(a/c) = 0.1$ and $(a/c) = 1.0$ for the two highest values of N_H , $5 \times 10^{24} \text{ cm}^{-2}$ (dotted) and 10^{25} cm^{-2} (dashed). The energy loss has again been normalized by the covering factor, (a/c) , so that the *shape* of the curves can be directly compared for different values of the covering factor. The curves for column densities lower than $5 \times 10^{24} \text{ cm}^{-2}$ in Fig. 6 do not show a discernible difference for different values of (a/c) .

We see from Fig. 6 that the total fractional energy loss functions for the *smallest* column densities are actually the *most* sensitive to Γ . For the lowest column density ($3 \times 10^{22} \text{ cm}^{-2}$), $CL[(a/c), N_H, \Gamma, E_U]$ varies by a factor of ~ 18 as Γ varies

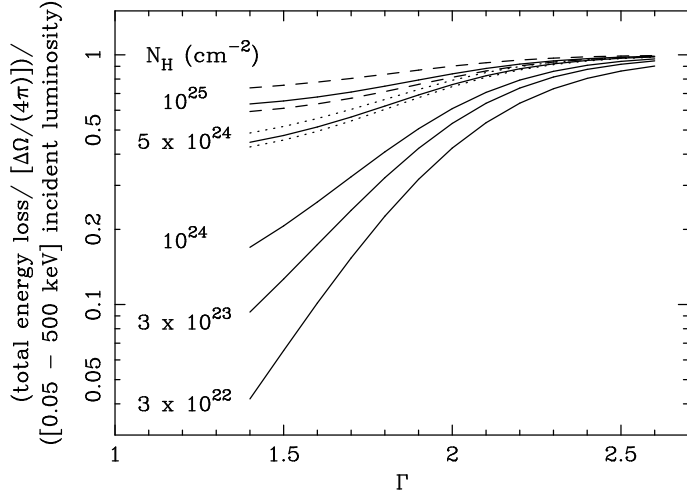


Figure 6. The total 0.05–500 keV integrated energy loss in the torus as a fraction of the total integrated energy in the same bandpass, as a function of the photon index of the incident power-law spectrum (Γ), for five different values of the torus equatorial column density, as indicated. The solid lines correspond to calculations with a covering factor, $[\Delta\Omega/(4\pi)] = (a/c)$ of 0.5. The dotted lines correspond, for $N_H = 5 \times 10^{24} \text{ cm}^{-2}$, to $(a/c) = 0.1$ (lower curve), and $(a/c) = 1.0$ (upper curve). The dashed lines correspond, for $N_H = 10^{25} \text{ cm}^{-2}$, to $(a/c) = 0.1$ (lower curve), and $(a/c) = 1.0$ (upper curve). All of the curves have been divided by the covering factor in order to facilitate a direct comparison of their *shape*.

between 1.4 and 2.6. However, for the highest column density (10^{25} cm^{-2}), $CL[(a/c), N_H, \Gamma, E_U]$ varies by only a factor of $\sim 1.3\text{--}1.7$ (depending on the covering factor) as Γ varies between 1.4 and 2.6. The reason for the larger sensitivity for smaller column densities is again that the dominant energy loss mechanism is absorption of low-energy photons in that regime. When the medium becomes Compton-thick, energy losses due to Compton downscattering dominate and multiple scatterings of high-energy photons tend to mitigate the sensitivity to Γ .

5 ENERGY LOSS AS A FRACTION OF THE OBSERVED TO INTRINSIC X-RAY LUMINOSITY RATIO

So far we have seen that of the three critical parameters of the system consisting of the X-ray reprocessor and its illuminating continuum (covering factor, N_H , and Γ), the energy deposited in the medium that is potentially available for reprocessing into infrared emission, is *least* sensitive to N_H . This already does not look promising for supporting the idea that the column density of the obscuring matter in AGNs could be constrained by the infrared emission. However, it is not the absolute infrared luminosity that is claimed in the literature to be the indicator of column density, but the ratio of the infrared luminosity to the *observed* X-ray luminosity. Since the latter has a strong dependence on the line-of-sight column density, it might be supposed that the ratio does in fact provide a good indicator of the column density. In order to address this question, we constructed a proxy for the infrared to X-ray luminosity ratio that is due to X-ray energy from the illuminating continuum deposited in the obscuring matter. Specifically, using our Monte Carlo results, we calculated the ratio of the total integrated fractional energy loss, $CL[(a/c), N_H, \Gamma, E_U]$ (see equation 3) to the ratio of the observed to intrinsic X-ray luminosity in the 2–10 keV band. We call this quantity $PX[(a/c), N_H, \Gamma]$, which can be written as

$$PX[(a/c), N_H, \Gamma] = \frac{CL[(a/c), N_H, \Gamma, E_U]}{[L_{\text{observed}}/L_{\text{intrinsic}}]_{2-10 \text{ keV}}}. \quad (4)$$

The quantity $CL[(a/c), N_H, \Gamma, E_U]$ represents only the energy *potentially* available for reprocessing into infrared emission so the quantity $PX[(a/c), N_H, \Gamma]$ is really an upper limit for a given set of parameters. However, this does not impact the basic test that we want to perform. We need to establish whether the ratio $PX[(a/c), N_H, \Gamma]$ is sensitive enough to N_H that it could distinguish between a Compton-thin and a Compton-thick AGN, despite the sensitivity of that ratio to Γ and to the covering factor. Deep X-ray survey data on AGNs do not have a sufficiently high signal-to-noise ratio to unambiguously determine Γ and (a/c) . Both parameters are highly model-dependent and degenerate with each other and with other model parameters for the signal-to-noise ratio that is typical of these deep survey AGN data (e.g., see discussion in Georgantopoulos et al. 2009). In the least constrained scenarios, X-ray spectroscopy is not even possible and inferences are made from X-ray hardness ratios alone, which carry an even greater degree of degeneracy (e.g., Polletta et al. 2006). We also note that covering factors deduced independently from other wavebands (e.g., the dust covering factor) are not necessarily equal to the X-ray

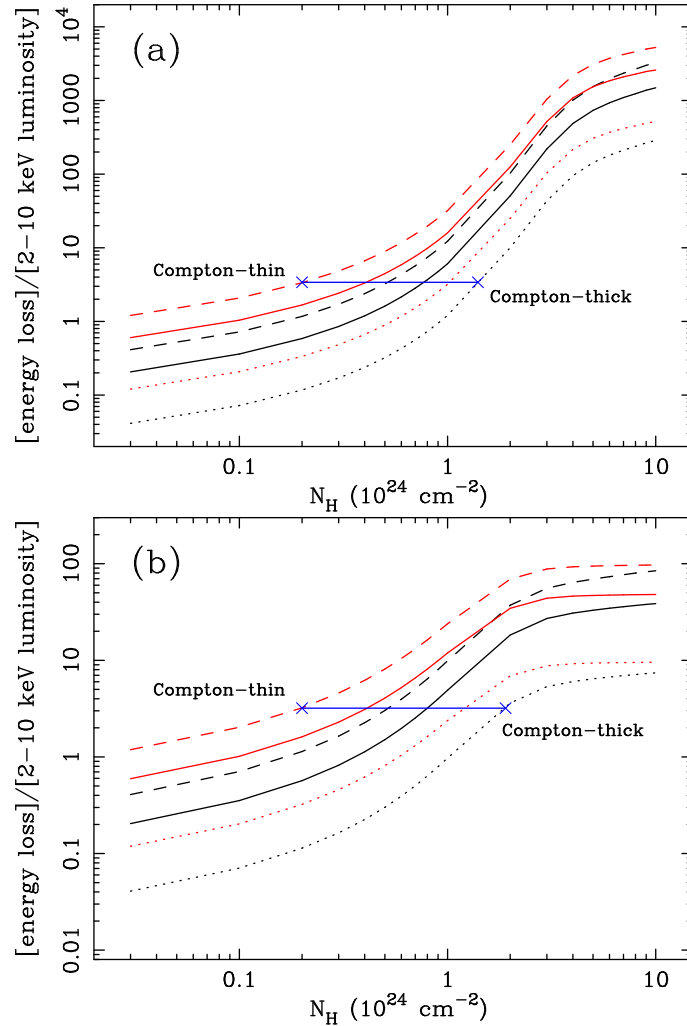


Figure 7. (a) The ratio of the total 0.05–500 keV integrated fractional energy loss as fraction of the 2–10 keV observed to intrinsic luminosity ratio, for a torus viewed edge-on, as a function of the column density. This ratio, $PX[(a/c), N_H, \Gamma]$ (see equation 4), is a proxy for the ratio of the fraction of the total X-ray luminosity that could be reprocessed into the infrared band, to the 2–10 keV X-ray observed to intrinsic luminosity ratio. Curves are shown for two values of the photon index of the incident power-law spectrum, $\Gamma = 1.9$ (black) and 2.5 (red). For each value of Γ , the curves are calculated for three values of the covering factor, $(a/c) = \Delta\Omega/(4\pi) = 0.1$ (dotted), 0.5 (solid), and 1.0 (dashed). The blue crosses joined by the blue horizontal line show that the proxy $PX[(a/c), N_H, \Gamma]$ is not a good indicator of N_H because, in this example, a Compton-thin source with $N_H = 2 \times 10^{23} \text{ cm}^{-2}$ and a Compton-thick source with $N_H = 1.4 \times 10^{24} \text{ cm}^{-2}$ have the same value of the proxy. This is because the dependence of the proxy on Γ and the covering factor can be greater than the dependence on N_H . (b) As (a) but this time the 2–10 keV luminosity included a power-law continuum due to scattering in an optically-thin zone surrounding the torus, corresponding to 1% of the direct (incident) X-ray continuum. The dependence of the proxy $PX[(a/c), N_H, \Gamma]$ on N_H is now even weaker. The blue crosses joined by the blue horizontal line show that a Compton-thin source with $N_H = 2 \times 10^{23} \text{ cm}^{-2}$ and a Compton-thick source with $N_H = 1.9 \times 10^{24} \text{ cm}^{-2}$ have the same value of the proxy.

covering factor. Therefore, in the absence of knowledge of Γ and the covering factor, if the theoretical ratio $PX[(a/c), N_H, \Gamma]$ is sufficiently sensitive to distinguish between a Compton-thin and a Compton-thick AGN, then the observed infrared to X-ray luminosity ratio *might* be a useful indicator of the column density. On the other hand, if $PX[(a/c), N_H, \Gamma]$ is not sufficiently sensitive to distinguish between a Compton-thin and a Compton-thick AGN, then the observed infrared to X-ray luminosity ratio *is not* an indicator of the column density.

Any additional infrared emission due to dust emission can only serve to *reduce* the usefulness of the observed infrared to X-ray luminosity ratio as an indicator of column density. There is at least one more complication. That is, we know from studies of bright AGNs that even in obscured sources the X-ray spectrum often shows an *unobscured* continuum component that is due to optically-thin electron scattering in an extended zone surrounding the central engine. Typically, this component can be characterized by a power-law continuum that has a luminosity that is $\sim 0.02\text{--}5\%$ of the direct (incident) continuum (e.g., Turner et al. 1997). However, in X-ray deep survey data the signal-to-noise ratio of the spectra for individual AGN is too poor to constrain this component. The resulting spectrum can then appear to have a smaller column density than that

which is actually obscuring the primary continuum if the optically-thin scattered continuum is not included in the model (and if it is, some assumptions have to usually be made about the pertinent parameters). In calculating the observed to intrinsic X-ray luminosity ratio in equation 4 we can include the optically-thin scattered continuum component, with its photon index and luminosity relative to the direct (incident) continuum as additional parameters. We note that the observed to intrinsic X-ray luminosity ratio depends on the orientation at which the torus is observed. In the following examples we will use an edge-on orientation because the the observed to intrinsic X-ray luminosity ratio is most sensitive to N_H when the torus is observed edge-on. Since we have already found that the energy losses are not very sensitive to N_H , we are looking for ways that $PX[(a/c), N_H, \Gamma]$ could recover some sensitivity to N_H and the edge-on orientation is the most appropriate for this purpose.

In Fig. 7 we show calculations of $PX[(a/c), N_H, \Gamma]$ from our Monte Carlo results. The curves in Fig. 7(a) were calculated with no optically-thin scattered continuum component and the curves in Fig. 7(b) were calculated with the inclusion of a continuum component with the same value of Γ as the primary continuum but with only 1% of the luminosity of the direct (incident) continuum. The curves shown in Fig. 7 were calculated for three values of the covering factor, $(a/c) = 0.1$ (dotted lines), $(a/c) = 0.5$ (solid lines), and $(a/c) = 1.0$ (dashed lines), and two values of Γ (1.9 and 2.5, corresponding to the black and red curves respectively).

We see from Fig. 7 that the sensitivity of $PX[(a/c), N_H, \Gamma]$ to the covering factor and Γ is still very strong and can in fact override the weak dependence of $PX[(a/c), N_H, \Gamma]$ on N_H . We also see that the effect of including the optically-thin scattered continuum, even at the level of 1%, significantly weakens the sensitivity of $PX[(a/c), N_H, \Gamma]$ to N_H . For the highest column densities, in the Compton-thick regime, we see that $PX[(a/c), N_H, \Gamma]$ drops by two orders of magnitude due to the optically-thin scattered continuum component, for the same values of Γ , (a/c) , and N_H .

In both Fig. 7(a) and Fig. 7(b) we illustrate one example in each case of a situation in which a Compton-thin AGN can give the same value of the ratio $PX[(a/c), N_H, \Gamma]$ as a Compton-thick AGN. The blue crosses joined by the blue horizontal lines show that the infrared to X-ray luminosity proxy is *not* a good indicator of N_H . In Fig. 7(a) the example shows that a Compton-thin source with $N_H = 2 \times 10^{23} \text{ cm}^{-2}$ and a Compton-thick source with $N_H = 1.4 \times 10^{24} \text{ cm}^{-2}$ have the *same* value of the proxy. In other words, a Compton-thin AGN with a steep spectrum and a high covering factor could give the same value of $PX[(a/c), N_H, \Gamma]$ as a Compton-thick AGN with a flatter spectrum and a smaller covering factor. In Fig. 7(b) the blue crosses joined by the blue horizontal line show that a Compton-thin source with $N_H = 2 \times 10^{23} \text{ cm}^{-2}$ and a Compton-thick source with $N_H = 1.9 \times 10^{24} \text{ cm}^{-2}$ have the *same* value of the proxy.

A general conclusion that can be drawn from Fig. 7 is that if we have a large sample of AGNs from a deep X-ray survey and examine the distribution of the ratio of observed infrared luminosity to X-ray luminosity, we could say that the AGNs with the highest value of that ratio *might* be Compton-thick candidates and/or heavily contaminated by dust emission. For the bulk of the AGNs in the distribution, the infrared luminosity to X-ray luminosity of a given AGN would tell us very little about the column density in the absence of information on the intrinsic X-ray continuum, the optically-thin scattered continuum, and the covering factor. This realization has already become apparent to Georgantopoulos et al. (2010) who have observationally identified some X-ray selected “infrared excess” AGNs that they call DOGs (Dust Obscured Galaxies) to be *Compton-thin*. Our theoretical results explain the reasons why the infrared luminosity to X-ray luminosity in AGNs is not a good indicator of the column density.

Our calculations have assumed a uniform distribution of matter, but the toroidal matter distribution may be clumpy (e.g., see Elitzur 2008, and references therein). In the optically-thin limit, a clumpy matter distribution will give the same results for the same *actual* covering factor, except that the covering factor is no longer an indicator of the solid angle subtended by the reprocessor at the X-ray source. An additional parameter, a filling factor, would be required to derive a relation between the solid angle and the covering factor. In the limit that each clump of matter is Compton thick, the total energy loss to the torus would be *less* than the corresponding uniform matter distribution with the same covering factor and mean column density (for the same incident X-ray continuum). This is because more lines-of-sight are available for X-ray photons to escape from the surface of a Compton thick clump after one or more scatterings (which may occur in more than one clump). Therefore the overall effect of clumpiness is to make the energy loss even less sensitive to the mean column density of the matter distribution because in the optically-thin limit the energy losses are the same but in the Compton-thick limit the losses are less for a clumpy distribution compared to a uniform matter distribution. Thus, the principal conclusions of the present paper still hold for a clumpy matter distribution.

6 SUMMARY

The aim of this paper was to investigate the theoretical foundation of the idea that the observed mid-infrared luminosity to X-ray luminosity ratio in AGNs that are found in deep X-ray surveys can be used as a proxy for the column density of obscuring matter, which therefore might be useful for identifying Compton-thick candidates. The basis for this is that energy lost by the X-ray continuum to the obscuring matter appears as reprocessed infrared emission. In order for the proxy to be viable a *minimal* requirement is that the energy losses due to absorption and Compton scattering in the obscuring matter

should be sensitive to the column density and *insensitive to other key physical parameters of the system*. By means of Monte Carlo simulations we found that the energy deposited in the obscuring matter and available for reprocessing into infrared emission has a sensitivity to the shape (steepness) of the incident X-ray continuum and the covering factor of the intercepted material that is far greater than the sensitivity to the column density. As a result, we found that the observed infrared to X-ray luminosity ratio for a Compton-thin AGN could be just as large as that for a Compton-thick AGN. The signal-to-noise ratio of the X-ray spectra of AGNs currently found in deep X-ray surveys is not sufficiently high to constrain the intrinsic X-ray spectrum and the covering factor of the reprocessor well enough to enable the infrared to X-ray luminosity ratio to be used as a reliable indicator of column density. If the infrared emission has a significant contribution from dust emission, for example due to starburst activity, the reliability of that indicator can only be worse. Our conclusion regarding the difficulty in the use of the mid-infrared to X-ray luminosity ratio for distinguishing between Compton-thin and Compton-thick AGNs is independent of the geometry of the obscuring matter in AGNs. It is also independent of the angular distribution of the intrinsic X-ray continuum emission. This is because the dominant energy loss mechanism changes from absorption to Compton scattering if the slope of the X-ray continuum is changed from having a power-law photon index of 2.5 to 1.5 (the typical range in AGNs), and this fact is independent of geometry. Further, the energy deposited in the obscuring matter trivially depends on the covering factor, and this fact is also independent of geometry.

Acknowledgments

Partial support (TY) for this work was provided by NASA through *Chandra* Award AR8-9012X, issued by the Chandra X-ray Observatory Center, which is operated by the Smithsonian Astrophysical Observatory for and on behalf of the NASA under contract NAS8-39073. Partial support from NASA grants NNX09AD01G and NNX10AE83G is also (TY) acknowledged.

REFERENCES

Alexander D. M., et al., 2008, ApJ, 687, 835
 Anders E., Grevesse N., 1989, *Geochimica et Cosmochimica Acta* 53, 197
 Ballantyne D. R., Papovich C., 2007, ApJ, 660, 988
 Bassani L., Dadina M., Maiolino R., Salvati M., Risaliti G., della Ceca R., Matt G., Zamorani G., 1999, ApJS, 121, 473
 Bauer F. E., Yan L., Sajina A., Alexander D. M., 2010, ApJ, 710, 212
 Bongiorno A., et al., 2010, A&A, 510, A56
 Cappi M., et al., 2006, A&A, 446, 459
 Comastri A., Setti G., Zamorani G., Hasinger G. 1995, A&A, 296, 1
 Daddi E., et al., 2007, ApJ, 670, 173
 Draper A. R., Ballantyne D. R., 2009, ApJ, 707, 778
 Elitzur M., 2008, New Astron., 52, 274
 Fiore F., et al., 2008, ApJ, 672, 94
 Fiore F., et al., 2009, ApJ, 693, 447
 Frontera F., et al., 2007, ApJ, 666, 86
 Georgantopoulos I., Akylas A., Georgakakis A., Rowan-Robinson M., 2009, A&A, 507, 747
 Georgantopoulos I., Georgakakis A., Rowan-Robinson M., Rovilos E., 2008, A&A, 484, 671
 Georgantopoulos I., Rovilos E., Xilouris E. M., Comastri A., Akylas A., 2010, A&A (in press) arXiv:1007.0350
 Ghisellini G., Haardt F., Matt, G., 1994, MNRAS, 267, 743
 Gilli R., Comastri A., Hasinger G., 2007, A&A, 463, 79
 Gilli R., Vignali C., Mignoli M., Iwasawa K., Comastri A., Zamorani G., 2010, A&A, 519, 92
 Hickox R. C., et al., 2007, ApJ, 671, 1365
 Horst H., Gandhi P., Smette A., Duschl W. J., 2008, A&A, 479, 389
 Ikeda S., Awaki H., Terashima, Y., 2009, ApJ, 692, 608
 Maiolino R., Salvati M., Bassani L., Dadina M., della Ceca R., Matt G., Risaliti G., Zamorani G., 1998, A&A, 338, 781
 Maiolino R., Shemmer O., Imanishi M., Netzer H., Oliva E., Lutz D., Sturm E., 2007, A&A, 468, 979
 Malizia A., Stephen J. B., Bassani L., Bird A. J., Panessa F., Ubertini P., 2009, MNRAS, 399, 944
 Malizia A., Stephen J. B., Bassani L., Bird A. J., Panessa F., Ubertini P., 2010, A&A (in press) arXiv:1002.4712
 Martínez-Sansigre A., et al., 2007, MNRAS, 379, L6
 Martínez-Sansigre A., Rawlings S., Lacy M., Fadda D., Marleau F. R., Simpson C., Willott C. J., Jarvis M. J., 2005, Nat, 436, 666
 Meléndez M., et al., 2008, ApJ, 682, 94
 Mullaney J. R., Alexander D. M., Huynh M., Goulding A. D., Frayer D. 2010, MNRAS, 401, 995
 Murphy K. D., Yaqoob T., 2009, MNRAS, 397, 1549 (MY09)
 Panessa F., Bassani L., Cappi M., Dadina M., Barcons X., Carrera F. J., Ho L. C., Iwasawa K., 2006, A&A, 455, 173
 Polletta M. d. C., et al., 2006, ApJ, 642, 673
 Reyes R., et al., 2008, AJ, 136, 2373
 Rowan-Robinson M., Valtchanov I., Nandra K., 2009, MNRAS, 397, 1326
 Setti G., Woltjer L., 1989, A&A, 224, L21
 Turner T. J., George I. M., Nandra K., Mushotzky R. F. 1997, ApJ, 488, 164
 Treister E., Urry C. M., Virani S., 2009, ApJ, 696, 110
 Tozzi P., et al., 2006, A&A, 451, 457
 Verner D. A., Ferland G. J., Korista K. T., Yakovlev D. G., 1996, ApJ, 465, 487

Verner D. A., Yakovlev D. G., 1995 *A&AS*, 109, 125
Vignali C., Alexander D. M., Gilli R., Pozzi F., 2010, *MNRAS*, 404, 48
Zakamska N. L., et al., 2003, *AJ*, 126, 2125